Geophysical & Astrophysical Fluid Dynamics

Publication details, including instructions for authors and subscription information:
http://www.tandfonline.com/loi/ggaf20

Reversals of a large-scale field generated over a turbulent background

B. Gallet [a], J. Herault [a], C. Laroche [a], F. Pétrélis [a] & S. Fauve [a]

[a] Laboratoire de Physique Statistique, Ecole Normale Supérieure, CNRS, 24 rue Lhomond, 75005 Paris, France

Version of record first published: 13 Feb 2012

To cite this article: B. Gallet, J. Herault, C. Laroche, F. Pétrélis & S. Fauve (2012): Reversals of a large-scale field generated over a turbulent background, Geophysical & Astrophysical Fluid Dynamics, 106:4-5, 468-492

To link to this article: http://dx.doi.org/10.1080/03091929.2011.648629

Geophysical and Astrophysical Fluid Dynamics
Vol. 106, Nos. 4–5, August–October 2012, 468–492

Taylor & Francis
Taylor & Francis Group

Reversals of a large-scale field generated over a turbulent background

B. GALLET, J. HERAULT, C. LAROCHE, F. PÉTRÉLIS and S. FAUVE*

Laboratoire de Physique Statistique, Ecole Normale Supérieure,
CNRS, 24 rue Lhomond, 75005 Paris, France

(*Received 26 July 2011; in final form 16 October 2011; first published online 13 February 2012*)

We present a study of several systems in which a large-scale field is generated over a turbulent background. These large-scale fields break a symmetry of the forcing by selecting a direction. Under certain conditions, the large-scale field displays reversals so that the symmetry of the forcing is recovered statistically. We present examples of such dynamics in the context of the dynamo instability, of two-dimensional turbulent Kolmogorov flows and of turbulent Rayleigh–Bénard convection. In these systems reversals occur respectively for the dynamo magnetic field, for the large-scale circulation generated by a periodic forcing in space and for the large-scale roll generated by turbulent thermal convection. We compare the mechanisms involved and show that their properties depend on some symmetries of the system and on the way they are broken.

Keywords: Dynamo; Convection; Turbulence; Reversals

1. Introduction

It is often believed that fully developed turbulent flows are statistically invariant under symmetry transformations of the forcing that generates them. Indeed, although the transition to turbulence involves successive bifurcations, each of them breaking some spatial or temporal symmetry, it is often observed that these symmetries are recovered in a statistical sense when the Reynolds number is increased further. The common belief is that strong turbulent fluctuations trigger random transitions between symmetric solutions and thus prevent the flow from staying in a regime with a broken symmetry. In other words, a strongly turbulent flow is expected to explore all the available phase space. However, it has been known for a long time that this is not so simple and that clear-cut transitions keep occurring within the strongly turbulent regime. The oldest example is provided by the drag crisis (see, for instance, Tritton 1977). The mean drag of a sphere or a cylinder in a turbulent flow drops suddenly for a critical value of the Reynolds number Re of order 10^5 (the pre-factor depending on surface properties). This corresponds to a transition where the mean flow pattern changes, the wake

*Corresponding author. Email: fauve@lps.ens.fr

Geophysical and Astrophysical Fluid Dynamics
ISSN 0309-1929 print/ISSN 1029-0419 online
http://dx.doi.org/10.1080/03091929.2011.648629

becoming narrower. Another example is related to Rayleigh–Bénard convection, i.e. the flow generated by heating from below a horizontal layer of fluid. It has been observed that for a Rayleigh number of order 10^6, i.e. roughly 1000 times larger than the critical Rayleigh number for the onset of convection, a large-scale flow is generated with a horizontal extension equal to the length of the container (Krishnamurti and Howard 1981). Von Karman swirling flows, i.e. flows generated in a cylindrical volume by the rotation of two co-axial disks, also display turbulent bifurcations. In the case of co-rotating disks, an axisymmetric mean flow with a strong axial vortex is observed. When the rotation rates are varied, this flow breaks axisymmetry, thus generating a roughly periodic modulation of the turbulent velocity field superimposed to turbulent fluctuations with $Re \sim 10^5$ (Labbé *et al.* 1996). In the case of disks counter-rotating at the same frequency, the forcing is symmetric with respect to a rotation of angle π around a radial axis in the mid-plane between the two disks (see below). It has been found that this symmetry can be broken through a bifurcation that occurs for Reynolds numbers in the range 10^5–10^6 (Ravelet *et al.* 2004).

There are a lot of other examples of transitions leading to broken symmetries in strongly turbulent flows. Bifurcations from a turbulent regime are therefore commonly observed. However, in contrast to bifurcations from stationary or space and time periodic flows, that are well documented and for which well-known techniques exist to handle both the linear stability problem and the weakly nonlinear bifurcated regime, the concept of bifurcation from a fully developed turbulent flow is more questionable even at the level of a clear-cut definition. In this respect, the dynamo effect in a liquid metal provides a very interesting example in which a magnetic field is generated by an instability process that occurs when the kinetic Reynolds number of the flow is usually larger than 10^6. Although the experiments involve some cost and technical difficulties, once the dynamo regime is reached, the dynamics of the magnetic field can be easily measured. Then, several interesting problems can be addressed. One of them is related to the possibility of anomalous scalings of the magnetic energy density above the dynamo threshold due to turbulent fluctuations (Pétrélis *et al.* 2007). Another one concerns the effect of turbulent fluctuations on the dynamics of the large-scale magnetic field. The symmetry $\boldsymbol{B}(\boldsymbol{r}, t) \to -\boldsymbol{B}(\boldsymbol{r}, t)$ of the equations of magnetohydrodynamics is spontaneously broken at the dynamo onset. Slightly above the threshold of a supercritically bifurcating dynamo, the magnetic energy density is much smaller than the kinetic energy density of turbulent fluctuations. However, turbulent fluctuations are not able to trigger a direct transition from B to $-B$ as would be observed in the naive analogy of a particle in a two-well potential in the presence of noise. In contrast, the VKS experiment, described in section 2, has shown that the reversal trajectories display very robust features that are not smeared out by turbulent fluctuations (Berhanu *et al.* 2007). In other words, the dynamics of the large-scale magnetic field involves only a few modes that look weakly coupled to the turbulent background, i.e. the reversal dynamics takes place in a low-dimensional phase space. Thus, the VKS dynamo provides an example in which a few magnetic modes are governed by a low-dimensional dynamical system although they occur on a strongly turbulent background at kinetic Reynolds number larger than 10^6.

Similar features are also observed in purely hydrodynamical models and the same problems can be addressed. This is the case in many geophysical and astrophysical flows where an oscillatory or a weakly chaotic behaviour can occur in flows at huge Reynolds numbers. Some climatic phenomena indeed display a characteristic feature of

low-dimensional chaos: well-defined patterns are observed despite the strongly fluctuating background. Examples are atmospheric blockings that can affect the climate on a time scale of several days (Ghil and Childress 1987) or El Niño events that occur every few years (Vallis 1986). The qualitative features of these phenomena have been often modelled using a few coupled variables such as mean temperature, wind or current. The quasi-biennial oscillation (QBO) provides a striking example of a large-scale almost cyclic reversing flow in the otherwise turbulent atmosphere. It is a roughly periodic oscillation in the strength and direction of the zonal (east-west) wind in the lower and middle stratosphere over the equator of the Earth's atmosphere. It has been observed for more than 50 years in climatological records. Its period fluctuates, the mean being slightly larger than 2 years. A reversal first appears at an altitude of roughly 40 km and then propagates downward at a rate of 1 km per month. Thus, these reversals are related to a downward drifting pattern. The QBO has been understood to arise from the interaction between upward-propagating waves, generated in the troposphere, and the mean zonal flow at upper levels where the waves are dissipated (for a review, see Baldwin *et al*. 2001). Reversals of large-scale flows driven on a turbulent background have also been observed in laboratory experiments, such as thermal convection (see Ahlers *et al*. 2009 for a review) and Kolmogorov flows, i.e. quasi-two-dimensional (2D) flows generated by forcing an array of counter-rotating vortices (Sommeria 1986). We first recall here old and recent observations related to bifurcations generating reversals of a magnetic field or of a mean flow in the presence of turbulent fluctuations and we discuss them in the framework presented above. Experimental results and models for reversals of the magnetic field are presented in section 2. Reversals of the large-scale flow generated by Kolmogorov forcing are studied in section 3. An experimental confirmation of Sommeria's results is provided and compared with a direct numerical simulation. A description of these reversals using a low-dimensional dynamical system is given and their main features are compared to the ones observed for the magnetic field. Reversals of the large-scale flow in Rayleigh–Bénard convection are considered in section 4. After recalling the results obtained in the literature, we present a new experiment showing that 3D perturbations can play an important role in the reversal process. Finally, we discuss the problem of reversals in relation to the phenomenon of drifting patterns and using the framework of amplitude equations. Thus, different types of bifurcations leading to reversals in this variety of systems can be easily identified. We conclude with a discussion on the relative contributions of the deterministic dynamics and of the turbulent fluctuations to reversals observed in strongly turbulent flows.

2. Reversals of the magnetic field generated in a fluid dynamo

2.1. *Dynamos, observations and laboratory experiments*

The dynamo process is an instability that converts mechanical work into electric current, i.e. magnetic energy. This has been used for a long time to generate electricity from the motion of solid rotators. Larmor (1919) proposed that in the Sun a similar instability could be operating that would convert kinetic energy of the flow of an electrically conducting fluid into magnetic energy. Nowadays it is strongly believed that most astrophysical objects (planets, stars, galaxies, etc.) generate a magnetic field

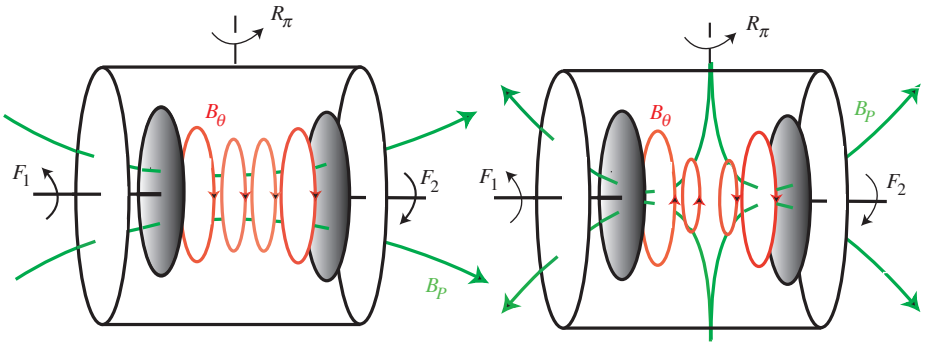

Figure 1. Sketch of the large scales of the eigenmodes of the VKS experiment. The two disks counter-rotate with frequency F_1 and F_2. Left: dipolar part of the magnetic mode. Right: quadrupolar part. Poloidal, B_P, and toroidal, B_θ, components are sketched.

through a dynamo instability (Moffatt 1978). Since the work of Brunhes (1906), it is known that the Earth's magnetic field keeps a roughly constant direction for long durations but from time to time it reverses and evolves toward the opposite direction. Reversals of the Earth's magnetic field have motivated a lot of studies ranging from paleomagnetism to numerical simulations of models of the Earth's interior (see, for instance, Dormy *et al*. 2000). The magnetic field of the sun also displays polarity reversals but they occur in a roughly periodic way every 11 years. Although direct numerical simulations are possible only in a parameter range orders of magnitude away from planetary or stellar dynamos, they have been able to display reversals of the magnetic field (Glatzmaier and Roberts 1995).

In the last decade, the first three experimental observations of fluid dynamos have been achieved in turbulent flows of liquid sodium: the Riga experiment (Gailitis *et al*. 2001), the Karlsruhe experiment (Stieglitz and Müller 2001) and the VKS experiment (Monchaux *et al*. 2007). The flow lines are strongly constrained by the geometry of the boundaries in the Riga and Karlsruhe experiments. The VKS experiment involves a von Karman swirling flow of liquid sodium generated by the rotation of two coaxial soft iron impellers at frequency F_1 (respectively F_2) inside a cylinder of aspect ratio of order one (see the sketch of figure 1). Thus, large-scale velocity fluctuations are important (comparable the mean flow) in the VKS experiment whereas they are small in the Riga and Karlsruhe experiments. Correspondingly, the geometry of the magnetic field generated in the Riga and Karlsruhe experiments is in very good agreement with the predictions made assuming that the mean flow is acting alone and discarding velocity fluctuations, whereas a similar assumption leads to strong disagreements for the VKS experiment. A detailed discussion of the dynamo generation observed in these three experiments is given in Pétrélis *et al*. (2007).

Above threshold, the VKS experiment displays a lot of secondary bifurcations to different dynamical regimes for the magnetic field whereas no secondary bifurcation has been reported in Karlsruhe or Riga. Some of these dynamical regimes involve reversals of the magnetic field (Berhanu *et al*. 2007). When the impellers counter-rotate with the same frequency F, a statistically stationary magnetic field is generated when F is large enough. Its mean value involves a dominant poloidal dipolar component, $\boldsymbol{B}_P$, along the axis of rotation, together with a related azimuthal component $\boldsymbol{B}_\theta$, as displayed in

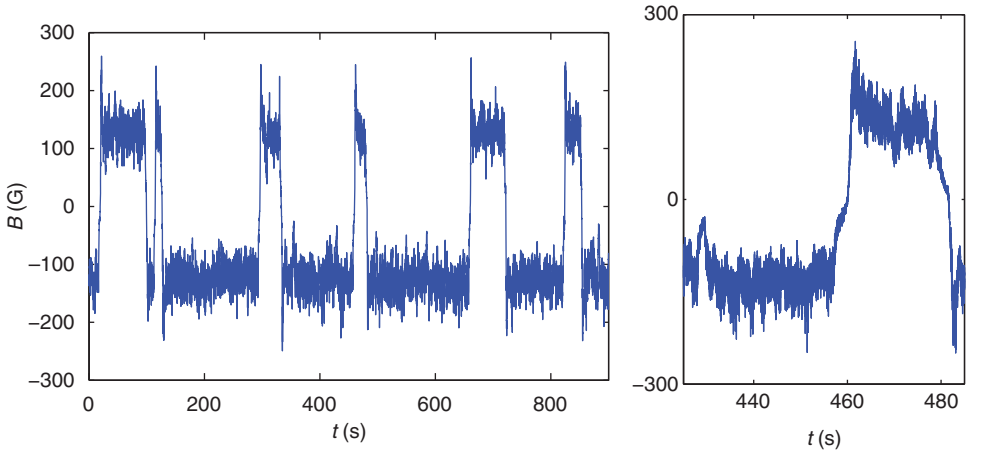

Figure 2. Left: Time series of the magnetic field measured in the VKS experiment in the regime of reversals. The two propellers counterrotate with different speeds. Right: zoom on two reversals and an excursion (data from Berhanu *et al.* 2007).

figure 1 (left). When the rotation frequencies are different, the magnetic field can display periodic or random reversals. A time series of the field in the regime of random reversals is shown in figure 2. The field fluctuates around some value for long durations, typically hundreds of seconds, and suddenly reverses within an ohmic diffusion time (roughly 1 s). Although the kinetic Reynolds number is large, $Re \sim 5 \times 10^6$ for these flows, it has been observed that low-dimensional dynamics of the magnetic field are not smeared out by strong turbulent fluctuations. In particular, all reversals involve the same transitional field morphology: the amplitude of the dipolar field first decreases. If it changes polarity, the amplitude increases on a faster time scale and then displays an overshoot before reaching its statistically stationary state. Otherwise, the magnetic field grows again with its direction unchanged. These features have been also observed in recordings of the Earth's magnetic field, the aborted reversals being often called excursions (Valet *et al.* 2005).

2.2. *Possible mechanisms for reversals of the magnetic field*

The first simple models of field reversals are illustrated by rotor disk dynamos following Rikitake (1958). Although these toy models strongly differ from the full MHD equations, it is possible to relate Rikitake equations with a simple model of an $\alpha - \omega$ dynamo (Moffatt 1978) or to obtain them by drastic truncation of the full MHD equations (Nozières 1978). One problem with truncated systems is that they usually describe dynamics that do not persist when higher modes are taken into account, thus making this approach questionable. A different and hopefully more realistic way to obtain a few coupled differential equations, is based on the assumption that several magnetic eigenmodes are competing above the dynamo threshold. It is then possible to write the corresponding normal forms. This has been done to describe the solar cycle and its slow modulation (Tobias *et al.* 1995, Wilmot-Smith *et al.* 2005). Knobloch and Landsberg (1996) consider a different model that involves two magnetic modes, a

dipolar and a quadrupolar one, both generated through a Hopf bifurcation. It has been also proposed to relate reversals to trajectories close to heteroclinic cycles that connect unstable fixed points $\pm\boldsymbol{B}$ (Armbruster *et al*. 2001). This provides a simple framework to describe separation of time scales between quasi-steady states with a given polarity, related to the slowing down of the system in the vicinity of a saddle point, and rapid reversal events. Melbourne *et al*. (2001) use this approach to describe the dynamics of Earth's magnetic field by writing amplitude equations for an equatorial dipole coupled to axial dipole and quadrupole. This model has heteroclinic cycles but no connection of states with opposite polarities except when additional coupling terms that break the symmetries are taken into account.

Another class of models uses external noise in order to model hydrodynamic fluctuations that trigger random transitions between the two states $\pm\boldsymbol{B}$. However, a dipolar mode alone subject to multiplicative noise does not lead to reversals even for large noise intensity. Random reversals occur only when damped modes coupled to the dipolar one are taken into account (Schmitt *et al*. 2001). Parker (1969) related the fluctuations of the velocity field required to generate a reversal to the number of cyclonic convective cells in Earth's core, that fluctuate both in number and position. He also suggested that an alteration of the meridional circulation could generate field reversals (Parker 1979). This has been observed in direct numerical simulations of the MHD equations in a rotating sphere (Sarson and Jones 1999).

Since 1995 (Glatzmaier and Roberts 1995), a lot of 3D numerical simulations of the MHD equations in a rotating sphere have been able to simulate a self-consistent magnetic field that displays reversals (see the review by Dormy *et al*. 2000). Although most relevant dimensionless parameters that can be achieved in direct simulations are orders of magnitude away from their values in Earth's core or laboratory experiments, thus making detailed comparisons questionable, several robust features related to the symmetry properties of reversals have been observed: a dipole–quadrupole interaction can be observed in the first reversals simulated by Glatzmaier and Roberts (1995) and the magnetic field has a quadrupolar symmetry at the transition (see their figure 2). This has been confirmed by the simulations of Sarson and Jones (1999) who also observed that reversals are triggered by the random emission of poleward light plumes, i.e. events that break the equatorial symmetry of the flow. Similar features have been observed by Wicht and Olson (2004). Li *et al*. (2002) also observed that "the dipole polarity can reverse only ... where the north-south symmetry of the convection pattern is broken". Nishikawa and Kusano (2008) showed that if the flow or the magnetic field is forced to remain equatorially symmetric, then reversals do not occur. Finally, it has been also proposed that reversals involve an interaction between dipolar and quadrupolar modes from an analysis of paleomagnetic data (McFadden *et al*. 1991).

2.3. *Mechanism for field reversals in the VKS experiment*

A striking feature of the VKS experiment is that time-dependent magnetic fields are generated only when the impellers rotate at different frequencies (Berhanu *et al*. 2007, Ravelet *et al*. 2008). It has been shown in Pétrélis and Fauve (2008) that this is related to the broken invariance under $\mathcal{R}_\pi$ when $F_1 \neq F_2$ (rotation of angle π around an axis in the mid-plane). Dipolar (resp. quadrupolar) modes of the magnetic field are displayed in figure 1 (left) (resp. right): a dipolar mode is changed into its opposite by $\mathcal{R}_\pi$, whereas a

quadrupolar mode is unchanged. When the impellers counter-rotate at the same frequency, the system is invariant under $\mathcal{R}_\pi$. Thus dipolar and quadrupolar modes are not linearly coupled. They become coupled when the impellers rotate at different frequencies such that the $\mathcal{R}_\pi$ symmetry is broken.

We assume that the magnetic field is the sum of a dipolar component with an amplitude D and a quadrupolar one, Q. This is justified when the thresholds of these two large-scale modes have similar values. We define $A = D + \mathrm{i}Q$ and we write an amplitude equation in the form of an expansion in powers of A and its complex conjugate $\bar{A}$. Taking into account the invariance $\boldsymbol{B} \to -\boldsymbol{B}$, i.e. $A \to -A$, we obtain

$$\dot{A} = \mu A + \nu \bar{A} + \beta_1 A^3 + \beta_2 A^2 \bar{A} + \beta_3 A \bar{A}^2 + \beta_4 \bar{A}^3 , \tag{1}$$

where we limit the expansion to the lowest order nonlinearities. In the general case, the coefficients are complex and depend on the experimental parameters. We obtain additional constraints on the coefficients when the impellers rotate at the same frequency because D and Q change in different ways under the transformation $\mathcal{R}_\pi$: $D \to -D, Q \to Q$, thus $A \to -\bar{A}$. We conclude that, in the case of exact counter-rotation, all the coefficients are real. Writing the equations for D and Q, we recover that the two modes are not linearly coupled as mentioned above. More generally, the real parts of the coefficients are even and the imaginary parts are odd functions of the frequency difference $f = F_1 - F_2$.

Let us denote the real (resp. imaginary) parts of the coefficients with subscript r (resp. i). In the counter-rotating case, the solution $\boldsymbol{B} = 0$ is unstable to a growing dipolar mode for $\mu_r > -\nu_r$ (we assume $\nu_r > 0$ such that the dipolar mode bifurcates first). When μ_r is increased, the quadrupolar mode also becomes linearly unstable for $\mu_r > \nu_r$. The linear stability analysis of the solution $A = 0$ gives the dispersion relation for the growth rate s

$$s^2 - 2\mu_r s + |\mu|^2 - |\nu|^2 = 0. \tag{2}$$

We have a stationary bifurcation for $|\mu| = |\nu|$ if $\mu_r < 0$, a Hopf bifurcation for $\mu_r = 0$ if $|\mu_i| > |\nu| > 0$, and a codimension-two bifurcation for $\mu_r = 0$ and $\mu_i^2 = |\nu|^2$.

Writing $A = R \exp \mathrm{i}\phi$, the stability of finite amplitude solutions can be studied in the phase approximation provided the amplitude R is slaved to the phase. We assume for simplicity that the nonlinear terms just saturate the amplitude without qualitatively changing the dynamics. The imaginary part of the linear part of (1) gives

$$\dot{\phi} = \mu_i - \nu_r \sin 2\phi + \nu_i \cos 2\phi. \tag{3}$$

The stationary solutions disappear via a saddle-node bifurcation when $\mu_i^2 = |\nu|^2$ and a limit cycle that corresponds to periodic reversals is generated. This occurs only if μ_i increases faster than ν_i when the $\mathcal{R}_\pi$ symmetry is externally broken. If $|\nu_i| > |\mu_i|$, the solutions remain stationary. A broken symmetry that induces $|\nu_i|$ much larger than $|\mu_i|$ has been found as a mechanism for hemispherical dynamos (Gallet and Pétrélis 2009). We emphasize that the location of the saddle-node bifurcation is modified when the nonlinear terms are taken into account.

The above phase approximation breaks down in the vicinity of the codimension-two point. Another type of bifurcation from stationary solutions to a limit cycle takes place in that case (Gambaudo 1985, Guckenheimer and Homes 1986). It is a subcritical Hopf bifurcation that can be easily discriminated from the previous scenario; the limit cycle

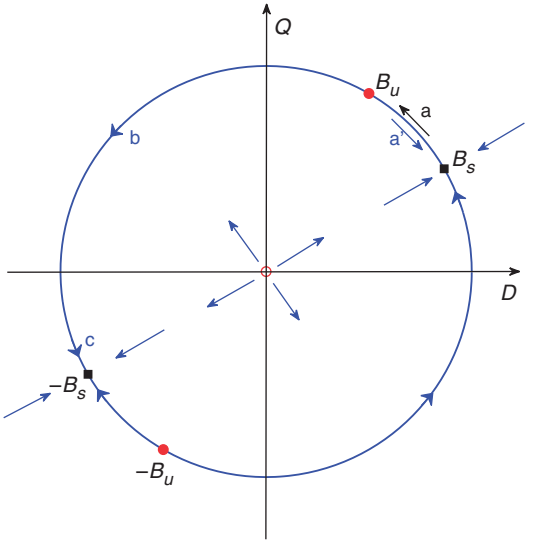

Figure 3. A generic saddle-node bifurcation in a system with the $\boldsymbol{B} \to -\boldsymbol{B}$ invariance: below threshold, fluctuations can drive the system against its deterministic dynamics (phase a). If the effect of fluctuations is large enough, this generates a reversal (phases b and c). Otherwise, an excursion occurs (phase a′).

appears with a finite period whereas the period diverges when it is generated through a saddle-node bifurcation. Stationary and oscillatory solutions coexist in some parameter range, thus this second scenario displays bistability. Both bifurcation types, saddle-node and subcritical Hopf, have been reported for the reversals of the magnetic field in the VKS experiment (Berhanu *et al.* 2009).

The effect of hydrodynamic fluctuations on reversals can be easily modeled by adding some noisy component to the coefficients of equation (1). We consider the scenario of reversals generated through a saddle-node bifurcation. Before the bifurcation, the solutions of equation (3) correspond to mixed dipolar-quadrupolar modes. The stable (resp. unstable) ones originate from $\pm D$ (resp. $\pm Q$) when $f=0$. These solutions are labeled $\pm B_s$ and $\pm B_u$ in figure 3. When a saddle-node bifurcation occurs for a larger value of f, the stable and unstable solutions collide by pairs and disappear (Pétrélis and Fauve 2008). A limit cycle is generated that connects the collision point, B_c, with its opposite.

This provides an elementary mechanism for field reversals. First, in the absence of fluctuations, the limit cycle generated at the saddle-node bifurcation connects $\pm B_c$. This corresponds to periodic reversals. Slightly above the bifurcation threshold, the system spends most of the time close to the two states of opposite polarity $\pm B_c$. Second, in the presence of fluctuations, random reversals can be obtained slightly below the saddle-node bifurcation. B_u being very close to B_s, even a fluctuation of small intensity can drive the system to B_u from which it can be attracted by $-B_s$, thus generating a reversal. Adding a noisy component to the coefficients of equation (1), we obtain random reversals displayed in figure 4 (left). The system spends most of the time close to the stable fixed points $\pm B_s$. We observe in figure 4 (right) that a reversal consists of two phases. In the first phase, the system evolves from the stable point B_s to the unstable point B_u (in the phase space sketched in figure 3). The deterministic part of the dynamics acts against this evolution and the fluctuations are the motor of the dynamics.

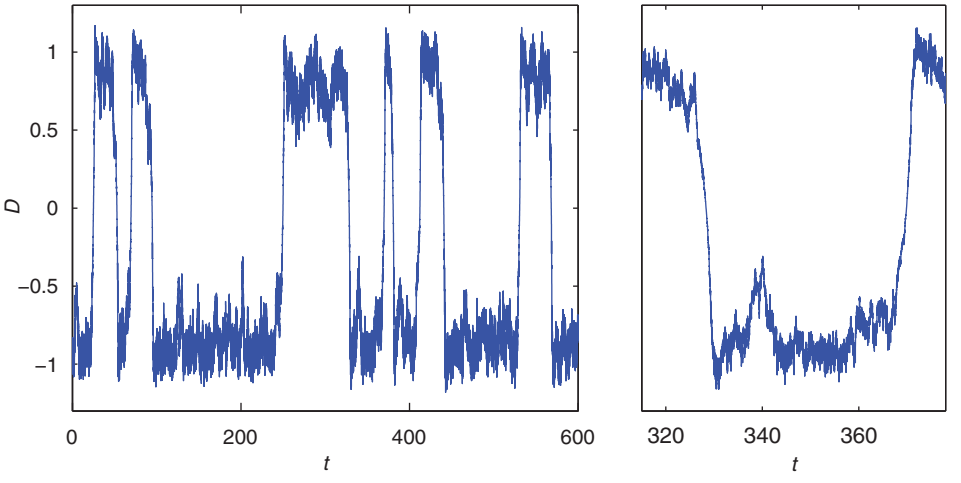

Figure 4. (left) Reversals of the magnetic field modelled by (1) with an extra noise term that takes into account the effect of the turbulent fluctuations. (right) Zoom on reversals and excursions.

This phase is thus slow. In the second phase, the system evolves from B_u to $-B_s$, the deterministic part of the dynamics drives the system and this phase is faster.

The behaviour of the system close to B_s depends on the local flow in phase space. Close to the saddle-node bifurcation, the position of B_s and B_u defines the slow direction of the dynamics. If a component of B_u is smaller than the corresponding one of B_s, that component displays an overshoot at the end of a reversal. In the opposite case, that component will increase at the beginning of a reversal. For instance, in the phase space sketched in figure 3, the component D decreases at the end of a reversal and the signal displays an overshoot. The component Q increases just before a reversal.

For some fluctuations, the second phase does not connect B_u to $-B_s$ but to B_s. It is an aborted reversal or an excursion in the context of the geodynamo. Note that during the initial phase, a reversal and an excursion are identical. In the second phase, the approaches to the fixed point differ because the trajectory that links B_u and B_s is different from the trajectory that links B_u and $-B_s$. In the case of figure 3, the dipole displays an overshoot at the end of a reversal and reaches smaller values during an excursion (see figure 4 right). By contrast the quadrupole exceeds its quasi-stationary value at the beginning of a reversal and reaches larger values during an excursion.

A direct numerical simulation of the dynamo generated by a flow driven in a sphere by two counter-rotating co-axial propellers (Gissinger *et al.* 2010) reproduced the main dynamical features of the VKS experiment. Reversals of the axial dipole occur only when the propellers are rotated at different rates. When the magnetic Prandtl number (P_m) is small enough, they involve an axial quadrupole and the dynamics of the dipolar and quadrupolar modes during a reversal is similar to the one observed in the experiment. Finally, although the flow in the VKS experiment strongly differs from the one in the Earth's core, dipolar and quadrupolar modes can be defined in both cases (using different symmetries) and the above model can be used to understand some features of the reversals of the Earth's magnetic field (Pétrélis *et al.* 2009).

2.4. *A dynamical system displaying random reversals of the magnetic field*

The above model for field reversals involves a planar dynamical system that describes the dynamics of the amplitude D (resp. Q) of the dipolar (resp. quadrupolar) component of the magnetic field. Random reversals are obtained only when multiplicative noise is taken into account in equation (1). A different approach is to model random reversals in a fully deterministic way by considering a dynamical system involving a third mode in addition to D and Q such that chaotic regimes become possible. This has been done by taking into account a zonal velocity mode V that breaks the $\mathcal{R}_\pi$ symmetry and thus couples D and Q (Gissinger *et al.* 2010). The equations for D, Q, V should satisfy the following symmetry constraints: $D \to -D$, $Q \to -Q$, $V \to V$ (invariance $\boldsymbol{B} \to -\boldsymbol{B}$ of the MHD equations) and $D \to -D$, $Q \to Q$, $V \to -V$ ($\mathcal{R}_\pi$ symmetry). The second invariance should be broken when the two propellers rotate at different frequencies. Keeping nonlinear terms up to quadratic order, we get

$$\dot{D} = \mu D - VQ, \tag{4a}$$

$$\dot{Q} = -\nu Q + VD, \tag{4b}$$

$$\dot{V} = \Gamma - V + QD. \tag{4c}$$

We consider that D and Q are close to their bifurcation thresholds (μ and ν small) but that V is linearly damped and we take its linear damping coefficient equal to 1 by an appropriate choice of the time scale. The coefficients of the nonlinear terms can be taken equal to ± 1 by scaling the amplitudes. Their relative signs have been chosen such that the solutions of (4) remain bounded when $\mu > 0$ and $\nu < 0$.

The dynamical system (4) with $\Gamma = 0$ occurs in many problems involving resonant waves and has been analysed in detail (Hughes and Proctor 1990). The $\mathcal{R}_\pi$ symmetry is externally broken when $\Gamma \neq 0$. In the VKS experiment, Γ represents the difference in rotation frequencies of the two propellers. A dynamical system similar to (4) has been obtained by Nozières (1978) using drastic truncation of the MHD equations. However, in that context both magnetic modes should be linearly damped ($\mu < 0$ and $\nu > 0$) thus strongly modifying the dynamics.

Numerical integration of (4) displays reversals of the components D and Q of the magnetic field for a wide range of parameters. A time recording is shown in figure 5. The modes D and Q are linearly coupled when $\Gamma \neq 0$. The basic mechanism is thus similar to the one previously described, but keeping the damped velocity mode V into the system (4) is enough to get chaotic attractors in the vicinity of the $\pm\boldsymbol{B}$ quasi-stationary states. Thus, the magnetic field fluctuates in the neighbourhood of one of the two states $\pm\boldsymbol{B}$ when the dynamo is statistically stationary. When μ is varied, the regime involving random reversals is obtained through a crisis mechanism (Grebogi *et al.* 1982), i.e. when the two symmetric attractors become connected in phase space. Compared to all previous deterministic models (see Pétrélis and Fauve 2010 for a review), the dynamical system (4) displays dynamical and statistical properties that are much closer to the ones observed in the VKS experiment or obtained by the direct numerical simulations at small P_m of Gissinger *et al.* (2010). In particular, the mean length of given polarity states is much longer than the duration of a reversal. In addition, the direct recordings of D or Q do not involve the growing oscillations characteristic of reversals displayed by the Rikitake (1958) or Lorenz (1963) systems but absent in dynamo experiments or in direct simulations. In contrast to previous

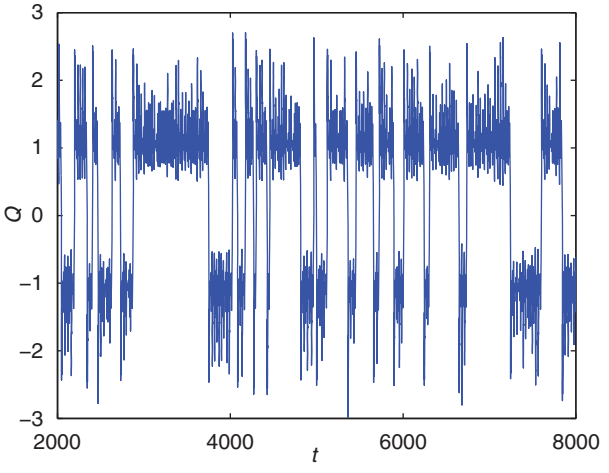

Figure 5. Numerical integration of the amplitude equations (4) from Gissinger *et al.* (2010). Time recording of the amplitude of the quadrupolar mode for $\mu = 0.119$, $\nu = 0.1$ and $\Gamma = 0.9$.

deterministic models, the probability density function of D is similar to the one obtained in experiments or direct simulations.

3. Large-scale circulation over a 2D turbulent flow

3.1. *Large-scale quasi-2D flows*

Rapid rotation or an externally applied strong magnetic field have been known since a long time to make flows 2D by inhibiting velocity gradients along the direction of the rotation axis or of the magnetic field (Chandrasekhar 1961). This situation is of obvious interest in the geophysical or astrophysical context where rotation can be important. The properties of turbulent flows strongly differ between these nearly 2D systems and the usual 3D ones. In 2D, it is well known that an inverse cascade tends to accumulate energy in the largest scales of the system. Early studies of periodically driven flows (Sommeria 1986, Tabeling *et al.* 1987) have shown that an array of vortices becomes unstable when the forcing is increased and that a large-scale circulation is generated in the whole system. This large-scale circulation is expected to display rich dynamics because it is coupled to the smaller scale turbulent fluctuations. Both the large-scale field and the fluctuations are therefore components of the same turbulent field, the velocity field. This differs from the former example in which reversals involve a field (the magnetic field) that is different from the turbulent velocity field.

3.2. *Reversals of the large-scale circulation in Kolmogorov flows: experiments and numerical simulation*

We have performed an experimental study of a Kolmogorov flow in a square layer of mercury of length $L = 12\,\text{cm}$ and depth $a = 1.6\,\text{cm}$. This layer is placed into a vertical

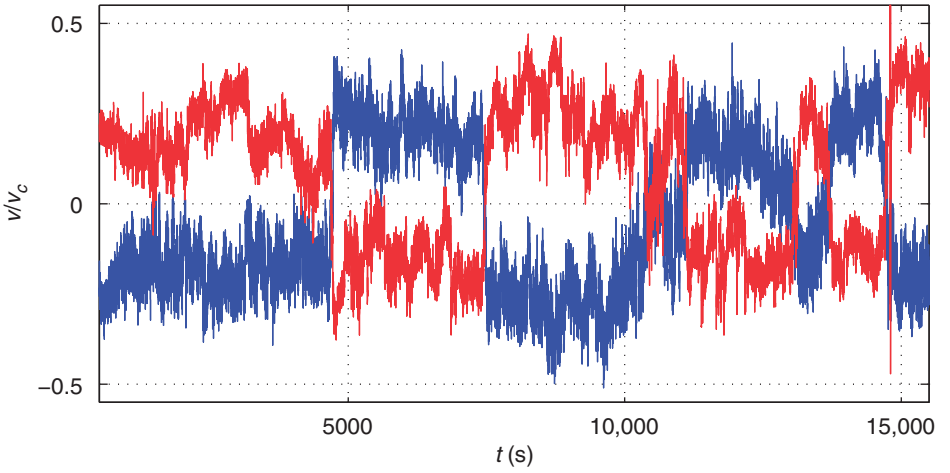

Figure 6. Time series of the velocity V/V_c where $V_c = (BI/(\rho a))^{1/2} \simeq 4.28\,\mathrm{cm\,s^{-1}}$ for $Rh = 37.7$ and $Re = 45000$. The two curves correspond to measurements located on opposite sides of the cell. The velocity is averaged between one centimeter and three centimeters away from the lateral wall.

magnetic field up to $B = 500\,\mathrm{G}$. An electric current I up to 40 A is injected in the fluid through 36 electrodes placed on a periodic square array. This current generates a Laplace force which drives the motion of the fluid. When the applied magnetic field is large enough, the flow is mostly 2D. At low current, a flow made of 36 counterrotating vortices is generated. For a large Reynolds number $Re = (BIL^2/(\rho a \nu^2))^{1/2}$ and large values of $Rh = (aI/(B\sigma\nu L^2))^{1/2}$, we observe that a large-scale circulation is generated either in the clockwise or counter-clockwise direction. When Rh is decreased, random reversals between these two directions of rotation are generated as already observed by Sommeria (1986). Let (x, y) be the coordinates measured from the lower left corner of the square. We present measurements of the x component of the velocity at position $(6, 2)\,\mathrm{cm}$ and $(6, 10)\,\mathrm{cm}$. The velocity is measured using Vives probes and is averaged over 2 cm. In figure 6, a time series is displayed in the regime of random reversals. The direction of the large-scale circulation remains constant for long durations, here larger than 1 h, and reverses in less than 100 s.

A numerical simulation of this experiment has been performed. When the magnetic field is strong enough, the flow is almost 2D and the stream function ψ obeys the 2D Navier–Stokes equation

$$\partial_t \Delta\psi + J(\Delta\psi, \psi) = -\frac{1}{Rh}\Delta\psi + \frac{1}{Re}\Delta^2\psi + 6\pi \sin(6\pi x)\sin(6\pi y). \tag{5}$$

The first term on the right-hand side is linear friction coming from the Hartmann layer on the bottom of the cell. The second one is the viscous term, and the last one mimics the electromagnetic forcing generated by the 6×6 electrodes. We solved this equation using a pseudo-spectral code with uniform time-stepping and stress-free boundary conditions (i.e. vanishing normal velocity and tangential constraint at the boundaries). The stream function is decomposed in the domain $(x, y) \in [0; 1]^2$ on the basis $(\sin(n\pi x)\sin(p\pi y))_{(n,p)\in\{1,\ldots,N\}^2}$. The linear terms are computed in Fourier space, while the nonlinear one is computed in real space. All the numerical runs described further

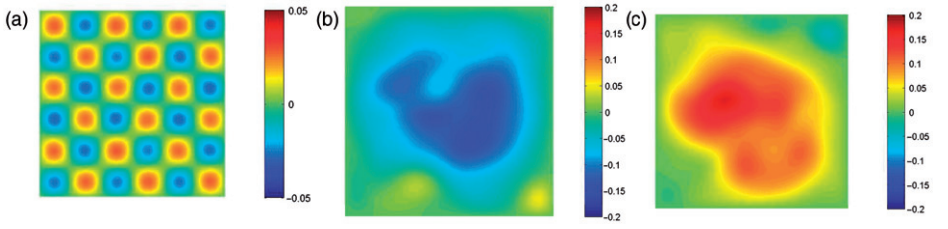

Figure 7. Stream function of the numerically computed solution of equation (5) for $Re = 2000$, $Rh = 55$, (a) snapshot at short time, the velocity field displays the same periodicity as the forcing. (b) and (c) are two snapshots displaying large-scale circulations of opposite signs. The large-scale flow has broken symmetries of the forcing. Under certain conditions, the circulation reverses from one state to the other.

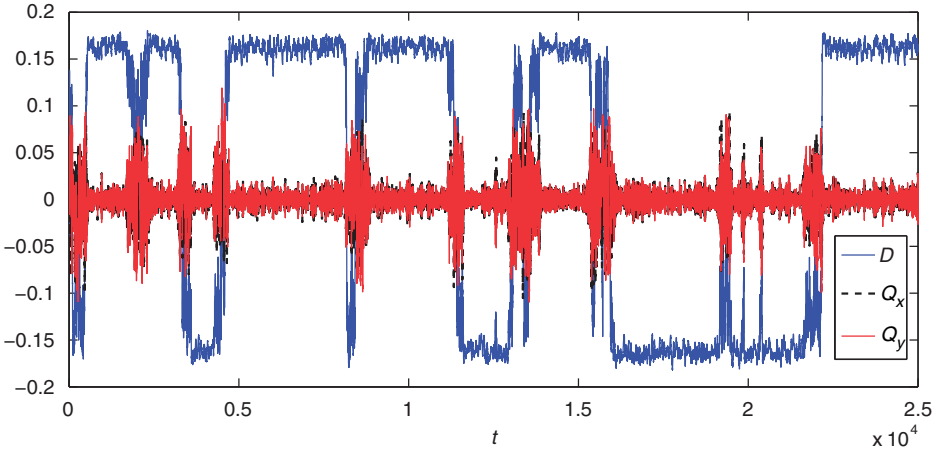

Figure 8. Time series of the amplitude of the large-scale circulation D and of two large-scale components Q_x and Q_y (see definition in the text) obtained numerically for $Rh = 65$ and $Re = 2000$.

were performed at $Re = 2000$ using 256 Fourier modes in each direction. We checked convergence: doubling this number of modes does not modify the numerical solution.

The velocity field obtained from direct numerical simulations is shown in figure 7. For weak damping coefficients, the laminar solution 7 (a) is unstable and a large-scale flow is generated. Two states are possible and are shown in figure 7 (b, c). We note that the forcing is invariant under the reflections with respect to the planes $x = L/2$ and $y = L/2$. We call $\mathcal{S}_x$ (respectively $\mathcal{S}_y$) these symmetries. The large-scale circulation thus breaks the symmetry of the forcing by selecting a direction of rotation. Under a critical value of R_h, reversals of this large-scale circulation are observed in the direct numerical simulations. An example of time series is shown in figure 8.

3.3. *A dynamical system displaying reversals of the large-scale circulation*

In the direct numerical simulation it is possible to identify the large-scale structures that are involved in the process of reversals. They can be decomposed into three

main components:

- The amplitude of the large-scale circulation is denoted as D and is defined here as the Fourier coefficient of $\sin(\pi x)\sin(\pi y)$ in the decomposition of the stream function.
- A second component, called Q_x, is the part of the large-scale flow that is quadrupolar in the x direction. It is even under $\mathcal{S}_x$ and odd under $\mathcal{S}_y$. It can be measured by the Fourier coefficient of ψ in $\sin(2\pi x)\sin(\pi y)$.
- A third component, called Q_y, is the part of the large-scale flow that is quadrupolar in the y direction. It is odd under $\mathcal{S}_x$ and even under $\mathcal{S}_y$. It can be measured by the Fourier coefficient of ψ in $\sin(\pi x)\sin(2\pi y)$.

We observe that reversals of D take place when Q_x and Q_y reach large values. In agreement with the experiment, no overshoot is seen at the end of the reversals.

In contrast to the reversals of the magnetic field close to the dynamo onset, we cannot invoke the proximity of a clear-cut bifurcation to justify a low order truncation. However at low friction (high Rh), energy accumulates in the lowest Fourier mode and the resulting global circulation displays little dynamics. When friction is increased, the accumulation of energy in the lowest Fourier mode is reduced and one of the two next Fourier modes increases. In order to obtain the minimal model that displays reversing dynamics, we assume that one can keep only the three large-scale modes described above. We note that the three components change differently under the different symmetries of the system. As already mentioned, D and Q_x are odd under $\mathcal{S}_y$ while Q_y is even. D and Q_y are odd under $\mathcal{S}_x$ while Q_x is even. A simple dynamical system that verifies these symmetries is

$$\dot{D} = -\nu D - Q_x Q_y \tag{6a}$$

$$\dot{Q}_x = Q_x - Q_y D - Q_x^3 \tag{6b}$$

$$\dot{Q}_y = \mu Q_y + D Q_x. \tag{6c}$$

It should come as no surprise that the equations for Q_x and Q_y are different. Indeed, the forcing breaks some of the square symmetries of the container. The forcing is not invariant to a rotation of angle $\pi/2$ around the center of the square. Note for instance the stagnation point at the center of the cell in the laminar solution displayed in figure 7(a) which shows that the x and y directions are not equivalent.

Compared to Hughes and Proctor (1990), the set of equations (6) contains an extra third-order nonlinearity in the second equation. A time series is represented in figure 9 for $\mu = 6$ and $\nu = 2.65$: the large-scale circulation D reverses randomly. As in the direct numerical simulations, the values of Q_x and Q_y increase during the reversals of D.

One should notice that the present problem maps onto the magnetic one in the following way: if we replace D, Q_y, and Q_x, respectively, by the amplitude of the dipolar magnetic component D, quadrupolar magnetic component Q, and equatorially-antisymmetric velocity component V, the symmetries $\mathcal{S}_x$ and $\mathcal{S}_y$ lead to the same constraints on the dynamical system than the invariance $\boldsymbol{B} \to -\boldsymbol{B}$ and the equatorial symmetry for the magnetic field of an astrophysical object. Therefore the system of equations (6) could describe the magnetic field of an astrophysical object as well, and leads to reversals of the magnetic dipole with no imposed equatorial-symmetry breaking. In this sense it is slightly different from model (2) in which the dynamics of V

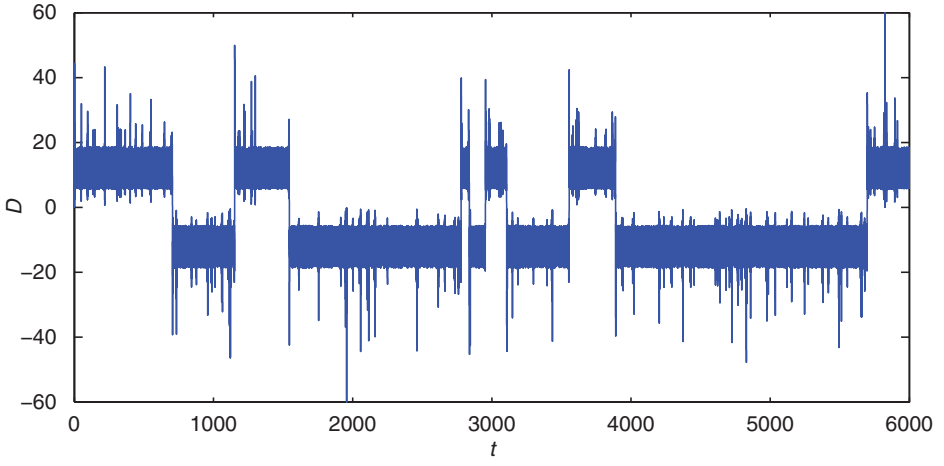

Figure 9. Time series of D solution of equations (6) in a regime of reversals ($\mu = 6$ and $\nu = 2.65$).

(corresponding to Q_x) results from an externally imposed broken symmetry and not from an instability of the large-scale velocity field that spontaneously breaks this symmetry. In these low-dimensional models, the system follows chaotic trajectories that wander in the basin of attraction associated to one polarity of the large-scale field or its opposite. There are thus two chaotic attractors that are symmetric to each other. As in the model described in section 2.4, reversals are generated through a crisis mechanism. In the regime of reversals each attractor has collided with the basin of attraction of the other one, and after a long duration the system escapes from one state toward its opposite.

4. Large-scale circulation in turbulent Rayleigh–Bénard convection

4.1. *Experiments on the dynamics of the large-scale circulation in Rayleigh–Bénard convection*

Rayleigh–Bénard convection is a canonical example of cellular instability. It is achieved by uniformly heating from below a horizontal layer of fluid. For small temperature difference ΔT across the layer of depth d, the fluid remains in a stable heat conducting state, with a linear temperature profile and no fluid motion. However, if the fluid's density is a decreasing function of temperature, the thermal gradient generates a density stratification with cold heavy fluid above warm light fluid. For sufficiently large temperature differences, the resulting buoyancy force overcomes dissipative effects due to kinematic viscosity, ν, and heat diffusivity, κ, causing less dense warmer fluid to rise and cooler fluid to sink. When the top and bottom boundaries have a thermal conductivity much higher than the one of the fluid, i.e. their temperatures are homogeneous, periodic parallel convection rolls of horizontal size comparable to d, result from the circulation of the fluid, when the Rayleigh number, $Ra = \alpha g \Delta T d^3/(\nu\kappa)$, is larger than a critical value, Ra_c (g is the acceleration of gravity, α is the coefficient of thermal expansion of the fluid). In the case of a large aspect ratio container (ratio of the

horizontal size L to the depth d), it has been observed by Krishnamurti and Howard (1981) that a large-scale horizontal shear flow of horizontal size L is generated for large enough values of Ra, roughly three orders of magnitude larger than Ra_c. For convenience, most high Rayleigh number experiments have been performed in cylindrical containers of aspect ratio one. In that case, the large-scale circulation evolves out of the cellular structure observed at convection onset without implying a secondary bifurcation and an associated broken symmetry. However, even in that simple case, this large-scale circulation displays dynamics that have been first related to flow reversals (see Ahlers *et al.* 2009 for a review of the early experiments and related models). It has been realised that, although simpler for the machine shop, the cylindrical geometry is not appropriate to study flow reversals. The convective pattern at onset and thus the large-scale circulation for large Ra indeed break the rotational invariance of the container. Thus, the dynamics primarily results from the azimuthal orientation of the large-scale circulation and the flow measured locally can vanish without necessarily implying a cessation of the whole large-scale circulation (Ahlers *et al.* 2009). Both reorientations and cessations of the large-scale circulation have been evidenced by recent direct numerical simulations (Mishra *et al.* 2011). They also displayed a quadrupolar temperature distribution during flow cessations (as opposed to the dipolar distribution resulting from the large-scale circulation). Thus, although different mechanisms are superimposed in the dynamics of large-scale circulation in cylindrical containers, flow cessations involve the competition between two large-scale modes with different symmetries, in striking analogy with the mechanism of reversals of the magnetic field proposed in 2.3.

Only a few studies of the dynamics of the large-scale circulation have been performed in parallelepipedic containers. Liu and Zhang (2008) reported a large-scale flow in an elongated box of aspect ratio 2.6 for $Ra > 10^7$ together with reversals but they provided a detailed study only with freely moving nylon spheres within the flow. Another experiment has been performed recently in a quasi-2D parallelepipedic container of aspect ratio one, and its results have been compared to direct numerical simulations of 2D convection (Sugiyama *et al.* 2010). Although the authors insist on the importance of corner flows superimposed to the large-scale diagonal circulation, a more pertinent observation is related to the change of symmetry of the large-scale flow observed during the reversal process. When the dipolar part of the large-scale flow vanishes, a quadrupolar structure is clearly visible (see their figure 1(b)). We also note that earlier 2D numerical simulations (Breuer and Hansen 2009) performed in a container of aspect ratio two also displayed the competition between two large-scale modes with different symmetries during the reversal process. Thus, it appears that, as for reversals of the magnetic field in the VKS experiment, reversals of the large-scale convective flow in the quasi-2D configuration also involve the competition between two large-scale modes with different symmetries. Another similarity between the convective and dynamo reversals is related to their occurrence in a finite interval range of the control parameters (Rayleigh and Prandtl numbers Ra, Pr or magnetic Reynolds numbers R_m). In both 2D numerical simulations of convection, it has been also reported that relatively small changes in the aspect ratio strongly modify the reversal dynamics and thresholds. This probably results from the inhibition of the mode with quadrupolar symmetry that is involved in the reversal process. Finally, the numerical simulations of Sugiyama *et al.* (2010) show that reversals disappear when the Prandtl number of the fluid is too small ($Pr \leq 0.7$) or too large. We will report below reversals in a cubic container of

mercury ($Pr \simeq 0.025$). Applying a horizontal magnetic field enables to make the flow more and more 2D by inhibiting velocity gradients along the direction of the magnetic field (Fauve *et al.* 1984). We will show that this strongly affects the reversal process.

4.2. *Dynamics of the large-scale circulation in a cubic container subject to a horizontal magnetic field*

We consider a cubic container of size $d = 45\,\mathrm{mm}$ filled with mercury of density $\rho = 13.5 \times 10^3\,\mathrm{kg\,m^{-3}}$, kinematic viscosity $\nu = 1.12 \times 10^{-7}\,\mathrm{m^2\,s^{-1}}$, thermal diffusivity $\kappa = 4.3 \times 10^{-6}\,\mathrm{m^2\,s^{-1}}$, specific heat $c_p = 138\,\mathrm{J\,kg^{-1}\,K^{-1}}$ and coefficient of thermal expansion $\alpha = 1.8 \times 10^{-4}\,\mathrm{K^{-1}}$. The side walls of the experiment are made of PVC while the top and bottom ones are copper plates. Water circulation through the upper copper plate maintains the upper temperature fixed. A constant heat flux F is imposed at the bottom boundary. The lower plate is covered with temperature probes which allow to determine the temperature difference between the bottom and the top plates ΔT and also to identify the spatial structure of the temperature field in the experiment. A horizontal magnetic field, B, up to 500 G can be applied perpendicularly to one of the sides of the cell. In figure 10, we display the Nusselt number $Nu = F/(\rho c_p \kappa \Delta T d)$ as a function of the Rayleigh number. In this regime of parameters, the magnetic field has little effect on the heat transport. For $\Delta T \simeq 48^\circ\mathrm{C}$, i.e. $Ra = 1.58 \times 10^7$, the variation of the Nusselt number is less than 4% when B is increased from 0 to 500 G corresponding to an interaction parameter, $N \sim (\sigma B^2/\rho)\sqrt{d/(\alpha g T)}$, smaller than 0.2.

In the absence of magnetic field, for Ra smaller than $Ra_r \simeq 4.3 \times 10^6$, the temperatures fluctuate around some constant value. In this regime, the larger scale of the convective pattern is a single roll that fills the whole cell. This roll is expected to be perpendicular to one of the sides of the cell and we have checked that its direction can be rotated by tilting the cell. However, no spontaneous change in the large scales of the temperature pattern is observed even for measurement durations larger than 24 h.

A change of behaviour is observed when Ra reaches Ra_r. The temperatures fluctuate for long durations around some value but from time to time, the whole temperature

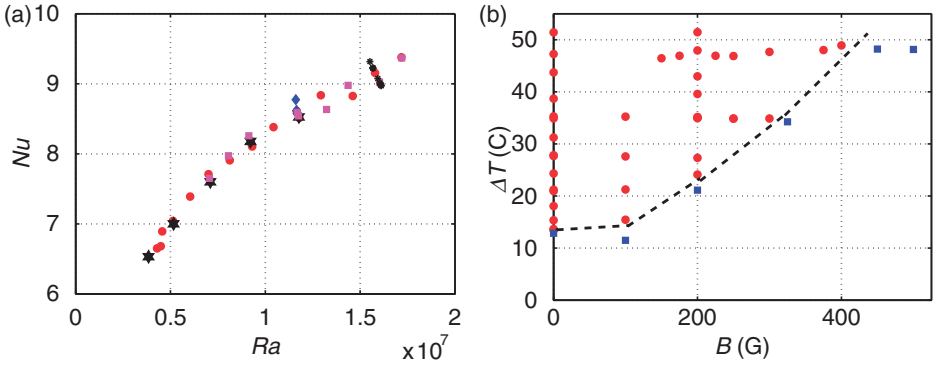

Figure 10. (a) Nusselt number as a function of the Rayleigh number for (○): $B = 0$, (⋆): $B = 100$ G, (□): $B = 200$ G, (∗): B varies from 0 to 500 G at $\Delta T \simeq 48^\circ$C, (◇): B varies from 0 to 325 G at $\Delta T \simeq 35^\circ$C. (b) Parameter space (B, ΔT). The blue squares correspond to stationary regimes. The red circles correspond to reversals of the large-scale circulation. The dashed line indicates the boundary between these two regimes.

pattern changes suddenly. Two time series of the temperature measured at opposite positions on the diagonal of the cell, 40 mm away from the corners, are displayed in figure 11. These large-scale modifications are separated by very long-time intervals, so that statistical properties can only be estimated. We have measured that the mean duration between these events decreases from more than 3 hrs to around 30 minutes when ΔT changes from 13.4 to 27.7°C.

Although the time series share common features with the ones of the reversals observed in the VKS experiment (figure 2) or in the 2D turbulent Kolmogorov flow (figure 6), we note that the evolution is more complicated: there are more than two stationary states and we can identify events where one of the temperatures changes with no noticeable evolution of the other one. Careful inspection of the evolution of several probes shows that the modifications of the large scales of the flow are associated to a rotation of the large-scale roll. This behaviour can be identified by considering the horizontal temperature gradients. In figure 12, we plot a cut in phase space

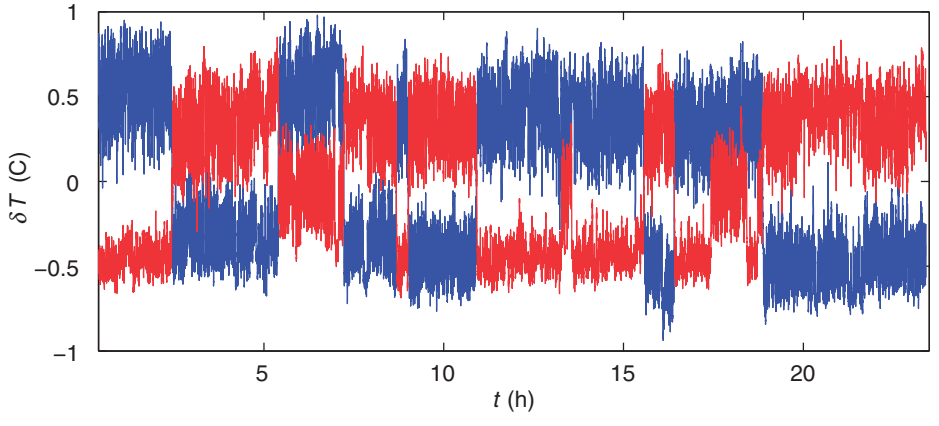

Figure 11. Time series of the temperature measured at two opposite corners of the lower plate for $B = 0$, $\Delta T = 15.4$°C and $Ra = 5.13 \times 10^6$. Measurement rate is 1/3 Hz and a sliding average over 10 measurements is performed to reduce fluctuations.

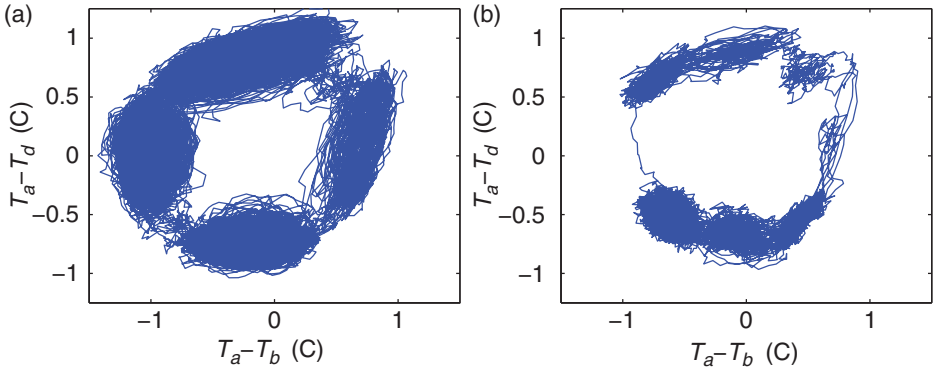

Figure 12. Projection of the phase space obtained from temperature differences: $T_a - T_d$ and $T_a - T_b$. (a) In the absence of applied magnetic field, same data as figure 11. (b) For $\Delta T = 48$°C, a magnetic field $B = 375$ G is applied parallel to the direction $a - b$.

$(T_a - T_b, T_a - T_d)$ where $T_a - T_b$ and $T_a - T_d$ are temperature differences measured along two perpendicular sides of the cell. The trajectories in phase space are roughly located along a circle. Between the changes of direction, the system fluctuates close to one of the four states that correspond to the roll rotation vector pointing towards one of the four lateral sides of the cell. Indeed, if a roll is aligned with the line $a-b$, then $T_a - T_b$ is roughly zero and the direction of rotation of the roll is given by the sign of $T_a - T_d$. The trajectory in phase space shows that the roll evolves from being perpendicular to one of the sides to being perpendicular to one of the two neighbouring sides. Its direction thus changes by $\pm 90^\circ$. In other words, the large-scale flow displays random changes of direction and reversals are obtained by the sequel of two changes of orientation in the same direction. This results in a rotation of 180° that amounts to change both the velocity and temperature perturbation fields to their opposite. Note, however, that in contrast to convection in a cylindrical container where a continuous rotation of the roll axis is possible, it is more pertinent here to understand the reversal dynamics as resulting from the competition of two perpendicular rolls. This emphasizes the analogy with the previous examples of sections 2 and 3 where a few large-scale modes are involved in the mechanism of reversals.

The obtained phase space clearly displays the four-fold symmetry of the experiment. This square symmetry can be broken applying a horizontal magnetic field. Measurements have been performed in which a field is applied parallel to the line joining a and b. In the parameter space displayed in figure 10(b), we observe that reversals disappear when the magnetic field is large enough. When reversals are observed in the presence of an applied magnetic field, the trajectories in phase space are modified. As displayed in figure 12(b), the two states corresponding to rolls perpendicular to the field ($T_a - T_d \simeq 0$) have lost stability: the system spends only a short time in these states. By contrast the system spends long durations in the vicinity of four new states. These states correspond to $T_a - T_b \simeq \pm(T_a - T_d)$ which in physical space means that a roll is aligned along the diagonal of the square. These observations result from the applied magnetic field that reduces the variations of the velocity along the direction of the field. The large-scale dynamics is thus modified by the following two effects: first, the rolls are preferably aligned along the magnetic field and rolls perpendicular to the field are expected to lose their stability; second, turbulence is reduced because fluctuations along the direction of the field are damped. These two effects explain that the pair of solutions perpendicular to the field turns unstable and ultimately that large-scale dynamics is suppressed.

From the point of view of low-dimensional modelling, figure 12 can be easily understood as phase dynamics. Indeed, in a cylindrical container, the system has rotational invariance. For a finite system, the axis of the large-scale roll rotates at no cost. If we assume that this rotational invariance is only weakly broken by the square geometry, the dynamics will still consist of rotations of the large-scale roll. The system is thus described by an equation for the orientation angle of the roll axis. The regime with $B = 0$ corresponds to a system with four stable fixed points. These stable points are located between four unstable states which are saddles (figure 13(a)). When a magnetic field is applied, a pair of stable solutions (transverse rolls) loses its stability. The four new states (diagonal rolls) that are observed can be described as two pairs of stable states that have been generated from a pitchfork bifurcation of the transverse rolls. The resulting phase space contains six nodes and, in-between, six saddles (figure 13(b)). A way to model the random dynamics of the large-scale flow is to consider that

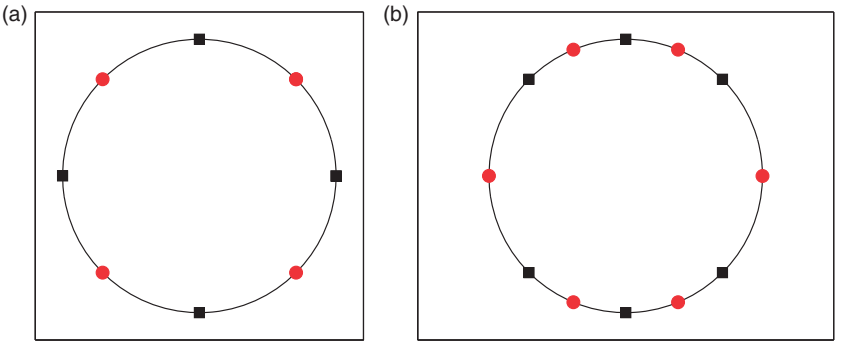

Figure 13. Phase space displaying stable solutions (□ black) and unstable solutions (○ red). (a) The four-fold symmetry is the one of the experiment in the absence of magnetic field. (b) In the case of an applied magnetic field, the two formerly stable solutions representing rolls perpendicular to the field are unstable and two pairs of new stable solutions (the diagonal rolls) are formed through a pitchfork bifurcation. Considering that turbulent fluctuations allow to evolve from a stable solution toward its neighbouring ones, both phase spaces represented in figure 12 can be reconstructed.

turbulent fluctuations act as noise that triggers transitions from one state to one of its neighbours.

As in the case of reversals of the magnetic field, the large-scale flow does not change sign directly under the influence of turbulent fluctuations (plumes, etc.). This transition always involves another (or several other) large-scale mode. In the case of square symmetry, perpendicular rolls are involved. When the square symmetry is broken by an external magnetic field, more complex mixed states are involved in the reversal process. For the Prandtl number of mercury, reversals are not observed above a critical value of the magnetic field. Finally, we note that the time series do not display a clear overshoot at the end of the reversals.

5. Discussion and conclusion

We have presented three examples of turbulent flows in which a field generated at large scale reverses. Some properties are common to the three systems. In all cases the large-scale field breaks a symmetry of the forcing and reversals allow the system to statistically recover this symmetry.

A clear separation of time scales exists between the duration of a reversal and the waiting time between reversals. Indeed, random reversals are rare events that are initiated when the system escapes from the basin of attraction of a fixed point. Once this phase has been completed, the evolution is fast because it does not require to reach a rarely visited domain in phase space.

During a reversal the whole field does not vanish. In particular, it is possible to identify large-scale structures that play a role in the dynamics and are visited by the system.

The three systems differ from the point of view of symmetries and in the way they are broken. The magnetic field and the large-scale circulation have two stable states while the large-scale roll in our convection experiment has four or six stable states. In the case of the experimental dynamo, one symmetry of the forcing is externally broken by

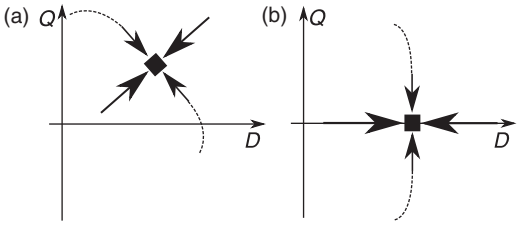

Figure 14. Phase space when two modes of opposite symmetries are involved. The smallest arrows are the eigenvectors of largest eigenvalue which define the less attracting direction. (a) When the symmetry is broken, the stationary state is a mixed mode and the asymptotic trajectories explore large values of D at the end of the reversal. (b) When the symmetry is not broken and the stationary state is a pure mode, the attracting directions are parallel to the $D=0$ and $Q=0$ axis. The trajectories are not enforced to explore large values of D.

rotating the two disks at different speeds. In the other two systems, one symmetry is spontaneously broken and this selects the direction of rotation of the roll's axis or the sign of the transitional two cell flow. These symmetry properties are responsible for the differences in shape of the reversals observed in the three systems. In particular, overshoots are observed only for some systems.

This feature can be understood in the case where the dynamics results from the competition between two modes of opposite symmetries, say D and Q. Then the evolution at the end of the reversals depends on whether the symmetry is broken or not. In the former case, the phase space in the vicinity of one of the stationary states has the form displayed in figure 14(a). The stationary state is a mixed mode. It is reached by trajectories that tend toward the less attracting direction (small arrow). The generic behaviour is then that the stationary value of D is exceeded either at the end or at the beginning of a reversal. The former case leads to an overshoot at the end of the reversals and is observed for the magnetic field in the VKS experiment as well as in the associated low-dimensional models (section 2). In contrast, when the symmetry is not broken and when the stationary state is a pure mode, say on the $Q=0$ axis, the phase space has the shape of figure 14(b). Studying the linear stability close to this state and taking into account the opposite symmetries of D and Q, the attracting directions are found parallel to the $D=0$ axis or to the $Q=0$ one. When the less attracting direction is the former one, the stationary state is reached by trajectories with constant D. The evolution in the vicinity of this state thus differs from the case where the symmetry is broken. In particular, the local behaviour close to the stationary state does not enforce the existence of an overshoot. This explains the shape of the reversals of the large-scale roll in Rayleigh–Bénard convection (section 4). Nevertheless, we point out that the phase space displayed in figure 14(b) is relevant only for the behaviour close to the stationary state for a system involving two modes. In particular, even if the symmetry is not externally broken, overshoots can be observed at the end of the reversals either because the dynamics involves more modes or because of the structure of the phase space far from the fixed point. For the reversals of the large-scale circulation generated over a Kolmogorov flow (section 3), we observe both types of reversals. For instance, in the direct numerical simulations reported here, overshoots are not observed in the time series of the amplitude of the large-scale circulation when a 6×6 vortex array is forced. In contrast, in the case of 2×4 vortices (not presented here), the reversals terminate with an overshoot. This last example shows that when the symmetry is not externally

broken, no prediction can be made for the existence of an overshoot, whereas when the symmetry is broken, the generic behaviour is that the reversals display an overshoot.

The geometry of the large-scale dynamics being governed by a low-dimensional dynamical system, we expect that reversals can also occur in laminar flows. This is indeed the case. Direct simulations of axisymmetric Rayleigh–Bénard convection in a cylindrical geometry (Tuckerman and Barkley 1988) as well as the weakly nonlinear analysis of the same system (Siggers 2003), have shown that the steady state observed above the convection onset can bifurcate to a travelling wave in which the number of rolls oscillates between two adjacent values. It has been emphasized that this transition to periodic behaviour is a symmetry-restoring bifurcation, as the states in the second half of the limit cycle are related to those of the first half by changing the sign of the velocity field (and accordingly of the temperature perturbation). A travelling spatially periodic pattern is indeed the simplest way to generate reversals of the flow measured at some location. This has been observed in direct numerical simulations of Rayleigh–Bénard convection with horizontal periodic boundary conditions (Paul *et al*. 2010). In that case, randomly occurring lateral shifts of the roll pattern by half a wavelength, lead to global flow reversals of the convective motion. These events are also observed in a finite interval range of Rayleigh number (although Ra is much smaller than in the presence of lateral boundaries). At first sight, one may believe that the presence of lateral boundaries deeply modifies the bifurcation mechanism leading to flow reversals but it is worth considering this analogy further. Drift instabilities of cellular patterns have been indeed observed in various experiments, such as Couette flow between two horizontal coaxial cylinders with a partly filled gap (Mutabazi *et al*. 1988), film draining (Rabaud *et al*. 1990), directional crystal growth (Simon *et al*. 1988), Faraday waves (Douady *et al*. 1989), etc. Some of them result from resonant 1:2 wave numbers (Proctor and Jones 1988). More generally, they occur when a secondary instability spontaneously breaks the reflection symmetry of the pattern which then travels in the direction related to this asymmetry (Coullet *et al*. 1989, Fauve *et al*. 1991, Caroli *et al*. 1992). If the reflection symmetry, say $x \to -x$, is externally broken, then one generically expects a spatially periodic pattern that breaks the translational invariance along the x-axis to drift along the x-axis at onset when the domain is infinite. This is easily understood in the framework of amplitude equations that amounts to describe a periodic pattern of wave number k in the form $A(t)\exp ikx + c.c. + \cdots$. $A(t)$ is a complex amplitude, $c.c$ stands for the complex conjugate of the previous term and the dots represent higher order terms in the vicinity of the bifurcation threshold. It is well known that the form of the equation for $\dot{A}$ in series of successive powers of A and $\bar{A}$ (the complex conjugate of A), results from the broken symmetries at the instability onset. If the system is invariant under the transformation $A \to -A$, this equation, up to leading order nonlinear terms, is identical to (1), where all the coefficients are complex numbers. If the system is translationally invariant along the x-axis, the amplitude equation should be invariant to a rotation in the complex plane, $A \to A \exp i\phi$, where ϕ is an arbitrary phase; thus $\nu = \beta_1 = \beta_3 = \beta_4 = 0$. If the system has parity invariance, $x \to -x$, which implies the invariance $A \to \bar{A}$ for the amplitude equation, then all the coefficients should be real. Thus, we get the usual amplitude equation that describes the stationary bifurcation of a homogeneous periodic pattern,

$$\dot{A} = \mu_r A + \beta_{2r}|A|^2, \tag{7}$$

where all the coefficients are real. When the parity invariance is externally broken, these coefficients generically have non-zero imaginary parts. When the imaginary part of μ, say μ_i, is non-zero, then the pattern is generated through a Hopf bifurcation and is thus a travelling wave that leads to periodic reversals of the flow at a given location. When the lateral boundaries are taken into account, translational invariance is externally broken and the leading order additional term that should be considered is $\nu\bar{A}$. This new term indeed tends to quench the phase of the pattern. The analysis is similar to the one in subsection 2.3. Two types of transition from a stationary pattern to travelling waves exist: one through a saddle-node bifurcation and the other through a subcritical Hopf bifurcation in the vicinity of the codimension-two point. Both bifurcation types, saddle-node and subcritical Hopf, have been reported for the axisymmetric convection problem (Siggers 2003) for which the externally broken reflection symmetry is related to the curvature of the rolls.

As mentioned above, drift bifurcations of cellular patterns also occur in a parity invariant system provided the reflection symmetry is spontaneously broken through a secondary bifurcation. This completes the analogy between drifting patterns in laminar flows and reversals of large-scale fields in the presence of turbulent fluctuations that can also occur as a result of an externally or a spontaneously broken symmetry.

In all the cases studied here, reversals occur through the connection in phase space between two solutions of opposite polarities and involve at least two large-scale modes. Small scale turbulent fluctuations thus do not play a major role in the geometry of reversals. They can of course trigger random reversals, for instance below a saddle-node bifurcation to a limit cycle. However, very similar random behaviours can be obtained with deterministic models involving three large-scale modes, so that it would not be so easy to determine the source of randomness in a natural system displaying reversals.

References

Ahlers, G., Grossmann, S. and Lohse, D., Heat transfer and large scale dynamics in turbulent Rayleigh–Bénard convection. *Rev. Mod. Phys.* 2009, **81**, 503–537.

Armbruster, D., Chossat, P. and Oprea, I., Structurally stable heteroclinic cycles and the dynamo dynamics. In *Dynamo and Dynamics, a Mathematical Challenge*, edited by P. Chossat, D. Armbruster and I. Oprea, Vol. 26, pp. 313–322, Nato Science Series II, 2001. (Kluwer Academic Publishers: Dordrecht).

Baldwin, M.P., Gray, L.J., Dunkerton, T.J., Hamilton, K., Haynes, P.H., Randel, W.J., Holon, J.R., Alexander, M.J., Hironta, I., Horinouchi, T., Jones, D.B.A., Kinnersley, J.S., Marquardt, C., Sato, K. and Takahashi, M., The quasi-biennial oscillation. *Rev. Geophys.* 2001, **39**, 179–229.

Berhanu, M., Monchaux, R., Bourgoin, M., Odier, Ph., Pinton, J.-F., Plihon, N., Volk, R., Fauve, S., Mordant, N., Pétrélis, F., Aumatre, S., Chiffaudel, A., Daviaud, F., Dubrulle, B. and Ravelet, F., Bistability between a stationary and an oscillatory dynamo in a turbulent flow of liquid sodium. *J. Fluid Mech.* 2009, **641**, 217–226.

Berhanu, M., Monchaux, R., Fauve, S., Mordant, N., Pétrélis, F., Chiffaudel, A., Daviaud, F., Dubrulle, B., Marié, L., Ravelet, F., Bourgoin, M., Odier, Ph., Pinton, J.-F. and Volk, R., Magnetic field reversals in an experimental turbulent dynamo. *Europhys. Lett.* 2007, **77**, 59001.

Breuer, M. and Hansen, U., Turbulent convection in the zero Reynolds number limit. *Europhys. Lett.* 2009, **86**, 24004.

Brunhes, B., Recherches sur la direction d'aimantation des roches volcaniques. *J. Phys. Theor. App.* 1906, **5**, 705–724.

Caroli, B., Caroli, C. and Fauve, S., On the phenomenology of tilted domains in lamellar eutectic growth. *J. Physique I* 1992, **2**, 281–290.

Chandrasekhar, S., *Hydrodynamic and Hydromagnetic Stability*, 1961. (Oxford: Clarendon Press).

Coullet, P., Goldstein, R.E. and Gunaratne, G.H., Parity-breaking transitions of modulated patterns in hydrodynamic systems. *Phys. Rev. Lett.* 1989, **63**, 1954–1957.

Dormy, E., Valet, J.-P. and Courtillot, V., Numerical models of the geodynamo and observational constraints. *Geochem. Geophys. Geosyst*. 2000, **1**, 2, C000062.
Douady, S., Fauve, S. and Thual, O., Oscillatory phase modulation of parametrically forced surface waves. *Europhys. Lett*. 1989, **10**, 309–315.
Fauve, S., Douady, S. and Thual, O., Drift instabilities of cellular patterns. *J. Physique II* 1991, **1**, 311–322.
Fauve, S., Laroche, C., Libchaber, A. and Perrin, B., Chaotic phases and magnetic order in a convective fluid. *Phys. Rev. Lett*. 1984, **52**, 1774–1777.
Gailitis, A., Lielausis, O., Platacis, E., Dement'ev, S., Cifersons, A., Gerbeth, G., Gundrum, T., Stefani, F., Christen, M. and Will, G., Magnetic field saturation in the Riga dynamo experiment. *Phys. Rev. Lett*. 2001, **86**, 3024–3027.
Gallet, B. and Pétrélis, F., From reversing to hemispherical dynamos. *Phys. Rev. E* 2009, **80**, 035302.
Gambaudo, J.M., Perturbation of a Hopf bifurcation by an external time-periodic forcing. *J. Diff. Eqns*. 1985, **57**, 172–199.
Ghil, M. and Childress, S., *Topics in Geophysical Fluid Dynamics: Atmospheric Dynamics, Dynamo Theory, and Climate Dynamics*, Applications in Mathematics and Science, Vol. 60, 1987. (New York: Springer Verlag).
Gissinger, C., Dormy, E. and Fauve, S., Morphology of field reversals in turbulent dynamos. *Europhys. Lett*. 2010, **90**, 49001.
Glatzmaier, G.A. and Roberts, P.H., A three-dimensional self-consistent computer simulation of a geomagnetic field reversal. *Nature* 1995, **377**, 203–209.
Grebogi, C., Ott, E. and Yorke, J.A., Chaotic attractors in crisis. *Phys. Rev. Lett*. 1982, **48**, 1507.
Guckenheimer, J. and Holmes, P., *Nonlinear Oscillations, Dynamical Systems and Bifurcations of Vector Fields*, 1986. (New York: Springer-Verlag).
Hughes, D.W. and Proctor, M.R.E., A low-order model of the shear instability of convection: chaos and the effect of noise. *Nonlinearity* 1990, **3**, 127–153.
Knobloch, E. and Landsberg, A.S., A new model for the solar cycle. *Mon. Not. R. Astron. Soc*. 1996, **278**, 294–302.
Krishnamurti, R. and Howard, L.N., Large-scale flow generation in turbulent convection. *Proc. Natl. Sci. USA* 1981, **78**, 1981–1985.
Labbé, R., Pinton, J.F. and Fauve, S., Study of the von Karman flow between coaxial corotating disks. *Phys. Fluids* 1996, **8**, 914–922.
Larmor, J., How could a rotating body such as the sun become a magnet? Report of 87th Meeting of British Association of Advance Sciences, Bournemouth, Sept. 9–13, pp. 159–160, 1919. (John Murray: London).
Li, J., Sato, T. and Kageyama, A., Repeated and sudden reversals of the dipole field generated by a spherical dynamo action. *Science* 2002, **295**, 1887–1890.
Liu, B. and Zhang, J., Self-induced cyclic reorganization of free bodies through thermal convection. *Phys. Rev. Lett*. 2008, **100**, 244501.
Lorenz, E., Deterministic non periodic flow. *J. Atmos. Sci*. 1963, **20**, 130–141.
McFadden, P.L., Merril, R.T. and McElhinny, M.W., Dipole/quadrupole family modeling of paleosecular variations. *J. Geophys. Res*. 1991, **93**, 11583–11588.
Melbourne, I., Proctor, M.R.E. and Rucklidge, A.M., A heteroclinic model of geodynamo reversals and excursions. In *Dynamo and Dynamics, a Mathematical Challenge*, edited by P. Chossat, *et al*., Vol. 26, pp. 363–370, Nato Science Series II, 2001. (Kluwer Academic Publishers: Dordrecht).
Mishra, P.K., De, A.K., Verma, M.K. and Eswaran, V., Dynamics of reorientations and reversals of large-scale flow in Rayleigh–Bénard convection. *J. Fluid Mech*. 2011, **668**, 480–499.
Moffatt, H.K., *Magnetic Field Generation in Electrically Conducting Fluids*, 1978. (Cambridge: Cambridge University Press).
Monchaux, R., Berhanu, M., Bourgoin, M., Moulin, M., Odier, Ph., Pinton, J.-F., Volk, R., Fauve, S., Mordant, N., Pétrélis, F., Chiffaudel, A., Daviaud, F., Dubrulle, B., Gasquet, C. and Marié, L., Generation of magnetic field by dynamo action in a turbulent flow of liquid sodium. *Phys. Rev. Lett*. 2007, **98**, 044502.
Mutabazi, I., Hegseth, J.J. and Andereck, C.D., Pattern formation in the flow between two horizontal coaxial cylinders with a partially filled gap. *Phys. Rev. A* 1988, **38**, 4752–4760.
Nishikawa, N. and Kusano, K., Simulation study of the symmetry-breaking instability and the dipole field reversal in a rotating spherical shell dynamo. *Phys. Plasma* 2008, **15**, 082903.
Noziéres, P., Reversals of the Earth's magnetic field: an attempt at a relaxation model. *Phys. Earth Planet. Interior* 1978, **17**, 55–74.
Parker, E.N., The occasional reversal of the geomagnetic field. *Astophys. J*. 1969, **158**, 815–827.
Parker, E.N., *Cosmical magnetic Fields*, 1979. (Oxford: Clarendon Press).
Paul, S., Kumar, K., Verma, M.K., Carati, D., De, A.K. and Eswaran, V., Chaotic travelling rolls in Rayleigh–Bénard convection. *Pramana J. Phys*. 2010, **74**, 75–82.
Pétrélis, F., Dormy, E., Valet, J.-P. and Fauve, S., Simple mechanism for the reversals of Earth's magnetic field. *Phys. Rev. Lett*. 2009, **102**, 144503.

Pétrélis, F. and Fauve, S., Chaotic dynamics of the magnetic field generated by dynamo action in a turbulent flow. *J. Phys.: Condens. Matter* 2008, **20**, 494203.
Pétrélis, F. and Fauve, S., Mechanisms for magnetic field reversals. *Philos. Trans. R. Soc. A* 2010, **368**, 1595–1605.
Pétrélis, F., Mordant, N. and Fauve, S., On the magnetic fields generated by experimental dynamos. *GAFD* 2007, **101**, 289–323.
Proctor, M.R.E. and Jones, C., The interaction of two spatially resonant patterns in thermal convection. Part 1. Exact 1:2 resonance. *J. Fluid Mech.* 1988, **188**, 301–335.
Rabaud, M., Michalland, S. and Couder, Y., Dynamical regimes of directional viscous fingering: spatiotemporal chaos and wave propagation. *Phys. Rev. Lett.* 1990, **64**, 184–187.
Ravelet, F., Berhanu, M., Monchaux, R., Aumaitre, S., Chiffaudel, A., Daviaud, F, Dubrulle, B., Bourgoin, M., Odier, Ph., Plihon, N., Pinton, J.-F., Volk, R., Fauve, S., Mordant, N. and Petrelis, F., Chaotic dynamos generated by a turbulent flow of liquid sodium. *Phys. Rev. Lett.* 2008, **101**, 074502.
Ravelet, F., Marié, L., Chiffaudel, A. and Daviaud, F., Multistability and memory effect in a highly turbulent flow: experimental evidence for a global bifurcation. *Phys. Rev. Lett.* 2004, **93**, 164501.
Rikitake, T., Oscillations of a system of disc dynamos. *Proc. Camb. Phil. Soc.* 1958, **54**, 89–105.
Sarson, G.R. and Jones, C.A., A convection driven geodynamo reversal model. *Phys. Earth Plan. Interior* 1999, **111**, 3–20.
Schmitt, D., Ossendrijver, M.A.J.H. and Hoyng, P., Magnetic field reversals and secular variation in a bistable dynamo model. *Phys. Earth Plan. Interior* 2001, **125**, 119–124.
Siggers, J.H., Dynamics of target patterns in low-Prandtl-number convection. *J. Fluid Mech.* 2003, **475**, 357–375.
Simon, A.J., Bechhoefer, J. and Libchaber, A., Solitary modes and the eckhaus instability in directional solidification. *Phys. Rev. Lett.* 1988, **61**, 2574–2577.
Sommeria, J., Experimental study of the two-dimensional inverse energy cascade in a square box. *J. Fluid Mech.* 1986, **170**, 139–168.
Stieglitz, R. and Müller, U., Experimental demonstration of a homogeneous two-scale dynamo. *Phys. Fluids* 2001, **13**, 561–564.
Sugiyama, K., Ni, R., Stevens, R.J.A.M., Chan, T.S., Zhou, S.-Q., Xi, H.-D., Sun, C., Grossmann, S., Xia, K.Q. and Lohse, D., Flow Reversals in Thermally Driven Turbulence. *Phys. Rev. Lett.* 2010, **105**, 034503.
Tabeling, P., Perrin, B. and Fauve, S., Instability of a linear array of forced vortices. *Europhys. Lett.* 1987, **3**(4), 459–465.
Tobias, S.M., Weiss, N.O. and Kirk, V., Chaotically modulated stellar dynamos. *Mon. Not. R. Astron. Soc.* 1995, **273**, 1150–1166.
Tritton, D.J., *Physical Fluid Dynamics*, 1977. (New York: van Nostrand Reinhold Company).
Tuckerman, L.S. and Barkley, D., Global bifurcation to traveling waves in axisymmetric convection. *Phys. Rev. Lett.* 1988, **61**, 408–411.
Valet, J.-P., Meynadier, L. and Guyodo, Y., Geomagnetic field strength and reversal rate over the past 2 Million years. *Nature* 2005, **435**, 802–805.
Vallis, G.K., El Nino: a chaotic dynamical system? *Science* 1986, **232**, 243–245.
Wicht, J. and Olson, P., A detailed study of the polarity reversal mechanism in a numerical dynamo model. *Geochem. Geophys. Geosyst.* 2004, **5**, Q03H10.
Wilmot-Smith, A.L., Martens, P.C.H., Nandy, D., Priest, E.R. and Tobias, S.M., Low-order stellar dynamo models. *Mon. Not. R. Astron. Soc.* 2005, **363**, 1167–1172.